HEAT-TRANSFER TESTS OF TWO SPACE SHUTTLE ORBITER CONFIGURATIONS AT MACH NUMBER 8

W. R. Martindale

ARO, Inc.

January 1974

Approved for public release; distribution unlimited.

VON KÁRMÁN GAS DYNAMICS FACILITY
ARNOLD ENGINEERING DEVELOPMENT CENTER
AIR FORCE SYSTEMS COMMAND
ARNOLD AIR FORCE STATION, TENNESSEE

NOTICES

HEAT-TRANSFER TESTS OF TWO
SPACE SHUTTLE ORBITER CONFIGURATIONS
AT MACH NUMBER 8

W. R. Martindale
ARO, Inc.

FOREWORD

The work reported herein was conducted at the Arnold Engineering Development Center (AEDC) under sponsorship of the National Aeronautics and Space Administration, Manned Spacecraft Center (NASA-MSC) for the University of Texas at Austin, under Program Element 921E-1.

The results of the tests presented were obtained by ARO, Inc. (a subsidiary of Sverdrup & Parcel and Associates, Inc.), contract operator of AEDC, Air Force Systems Command (AFSC), Arnold Air Force Station, Tennessee. These tests were conducted on August 25 and 28 and September 28, 1972, under ARO Project Number VAO24, and the final data package was completed on October 12, 1972. The manuscript was submitted for publication on December 14, 1972.

This technical report has been reviewed and is approved.

JIMMY W. MULLINS
Lt Colonel, USAF
Chief Air Force Test Director, VKF
Directorate of Test

FRANK J. PASSARELLO
Colonel, USAF
Director of Test

ABSTRACT

Heat-transfer tests were conducted on two Space Shuttle configurations at Mach number 8 to investigate the effects of nose geometry on windward and leeward heating and boundary-layer transition. Free-stream Reynolds number based on model length was varied from 1.5 to 7.5 million at angles of attack from 20 to 50 deg. Windward centerline heating rates were in general agreement with calculated values except for laminar rates downstream of the wing/body junction. Differences in the location of the beginning of transition and the length of the transition zone were observed for the two configurations, but it was not clear whether variation in nose shape per se or the abrupt cross-sectional change from the nose to the aft fuselage and wing was the controlling factor.

CONTENTS

APPENDIXES

I. ILLUSTRATIONS

Figure

NOMENCLATURE

b   Model skin thickness, ft

c_p Specific heat, Btu/lbm-°R

h   Heat-transfer coefficient, $\dot{q}/(T_o - T_w)$, Btu-ft^2-sec-°R

L   Axial length of model, in.

M   Mach number

p   Pressure, psia

p_o' Stagnation pressure downstream of a normal shock, psia

$\dot{q}$ Heat-transfer rate, Btu/ft^2-sec

Re_e Unit Reynolds number based on edge conditions, ft^{-1}

$Re_{e,\bar{x}}$ Reynolds number based on edge conditions and surface distance

$Re_{\infty,L}$ Free-stream Reynolds number based on length

T   Temperature, °R

t   Time, sec

w   Model skin density, lbm/ft^3

x   Axial distance from model nose, in.

$\bar{x}$ Surface distance from the model nose in the axial direction, in.

α Angle of attack, deg

γ Specific heat ratio for air, 1.40

θ_s Angle between free-stream velocity vector and tangent to local bow shock, deg

σ Angle between model axis and local tangent to model surface, deg

SUBSCRIPTS

e   Edge conditions

i   Initial conditions

ℓ Local conditions

o   Stilling chamber conditions

ref   Heat-transfer parameter based on Fay-Riddell theory and a 1-ft nose radius scaled down to the model scale (0.019 ft)

TB   Beginning of transition

TE   End of transition

w   Wall conditions

θ Momentum thickness, ft

∞ Free-stream conditions

SECTION I
INTRODUCTION

Optimum design of the thermal protection system for the Space Shuttle orbiter depends largely on the accurate prediction of heating rates to be experienced by the vehicle in flight. The heating rate predictions, in turn, depend largely upon ground test data and the attendant procedures used to extrapolate the data to flight conditions. Subtle geometric variations may have significant effects on both the ground test data and the flow models used to extrapolate the data to flight conditions.

The present tests were undertaken to study the effects of nose geometry on windward and leeward heating rates and boundary-layer transition on a representative Space Shuttle orbiter configuration. Two nose shapes were investigated using a common wing and afterbody. The tests were conducted in the Hypersonic Wind Tunnel (B) of the von Kármán Gas Dynamics Facility (VKF) at Mach number 8, and the thin-skin thermocouple technique was used for obtaining heating rates. Angle of attack was varied from 20 to 50 deg at free-stream Reynolds numbers from 1.5 to 7.5 million based on model length.

SECTION II
APPARATUS

2.1 MODELS

The overall model dimensions and wing, fuselage, and canopy details were provided by the Manned Spacecraft Center (MSC), whereas the nose configurations were designed by the University of Texas at Austin. A model drawing is shown in Fig. 1, Appendix I, and photographs are shown in Figs. 2 and 3.

The model noses ($x/L \leq 0.3$) were designed so that the surface geometry could be described by analytic functions. Two elliptical planforms were used with a common profile (see Fig. 1). Nose cross sections are shown in Fig. 4. The aft fuselage and wing geometry ($x/L \geq 0.4$) were common to both, requiring abrupt change in cross section in the region $0.3 \leq x/L \leq 0.4$.

The model nose and lower fuselage surfaces were electroformed in one piece from nickel, providing a continuous lower surface from nose to tail. The upper fuselage was also constructed of electroformed nickel. Nominal thickness of the electroformed parts was 0.035 in. The wings were machined from solid 17-4 PH stainless steel.

2.2 WIND TUNNEL

Tunnel B is a continuous, closed-circuit, variable density wind tunnel with an axisymmetric contoured nozzle and a 50-in.-diam test section. The tunnel can be operated at a nominal Mach number of 6 or 8 at stagnation pressures from 20 to 300 and 50 to 900 psia, respectively, at stagnation temperatures up to 1350°R. The model can be

injected into the tunnel for a test run and then retracted for model cooling or model changes without interrupting the tunnel flow. A description of the tunnel may be found in Ref. 1.

2.3 INSTRUMENTATION

Each of the two configurations was instrumented with 103 Chromel®-Alumel® thermocouples, of which 98 were used. Only the fuselage was instrumented. Thermocouple locations are shown graphically in Fig. 4.

Thermocouple outputs were recorded on magnetic tape at the rate of 20 times per second from the start of model injection until about 4 sec after the model reached tunnel centerline.

<div align="center">

SECTION III
PROCEDURE

</div>

3.1 TEST CONDITIONS

A complete test summary is given below. Each configuration was tested at all the conditions listed except as noted.

M_∞	p_o, psia	T_o, °R	$Re_{\infty,L}$	a, deg
8.01	863	1345	7.48×10^6	20,30,40,50
8.00	725	1323	6.40×10^6	30
7.98	600	1312	5.46×10^6	30
7.97	420	1287	3.92×10^6	20,25,30,35, 40,50
7.96	300	1275	2.86×10^6	30
7.92	150	1220	1.45×10^6	20*,30,35**, 40,50

*Oil flow, Configuration UTN7 only
**Oil flow only, both configurations

Uncertainties in the basic flow parameters p_o, T_o, and M_∞ were estimated from repeat calibrations of the instruments and from repeatability and uniformity of the test section flow during tunnel calibration. The individual contributions of these uncertainties were propagated through the appropriate flow equations to obtain the uncertainties of calculated parameters.

Approximate uncertainties in tunnel flow parameters are shown as follows:

Parameter	Uncertainty, Percent
p_o	±0.5
T_o	±1.0
M_∞	±0.3
h_{ref}	±1.0
$Re_{\infty,L}$	±2.0

3.2 DATA REDUCTION

The reduction of thin-skin thermocouple data normally involves only the calorimetric heat balance, which, in coefficient form, is

$$h = wbc_p\left(\frac{dT_w/dt}{T_o - T_w}\right) \qquad (1)$$

Radiation and conduction losses are neglected in this heat balance, and data reduction simply requires evaluation of dT_w/dt from the temperature-time data and determination of model material properties. For the present tests, radiation effects were negligible; however, conduction effects were significant in several regions of the models. To permit identification of these regions and improve evaluation of the data, the following procedure was used.

Separation of variables and integration of Eq. (1), assuming constant w, b, c_p, and T_o, yields

$$\frac{h}{wbc_p}(t - t_i) = \ln\left(\frac{T_o - T_{wi}}{T_o - T_w}\right) \qquad (2)$$

Since h/wbc_p is a constant, plotting $\ln[(T_o - T_{wi})/(T_o - T_w)]$ versus time will give a straight line if conduction is negligible. Thus, deviations from a straight line can be interpreted as conduction effects.

The data were evaluated in this manner, and generally a reasonably linear portion of the curve could be found for all thermocouples. A linear least squares curve fit of $\ln[(T_o - T_{wi})/(T_o - T_w)]$ versus time was applied to the data beginning at the time when the model reached uniform flow and extending for a time span which was a function of the heating rate, as shown below:

Range	Number of Points
$dT_w/dt > 32$	5
$16 < dT_w/dt \leq 32$	7
$8 < dT_w/dt \leq 16$	9
$4 < dT_w/dt \leq 8$	13

3

Range	Number of Points
$2 < dT_w/dt \leq 4$	17
$1 < dT_w/dt \leq 2$	25
$dT_w/dt < 1$	41

In general, the time spans given above were adequate to keep the evaluation of the right-hand side of Eq. (2) within the linear region. Strictly speaking, the value of c_p is not constant, as assumed, and the relation

$$c_p = 0.1467 - (2.173 \times 10^{-4})\,T_w - (3.367 \times 10^{-7})\,T_w^2$$
$$- (1.332 \times 10^{-10})\,T_w^3, \; Btu/lbm\text{-}°R \tag{3}$$

which was obtained from a least squares fit of the specific heat data for nickel tabulated in Ref. 2 was used with the value of T_w at the midpoint of the curve fit. The maximum variation of c_p over any curve fit was less than one percent; thus, the assumption of constancy was not grossly violated. A constant 555 lb_m/ft^3 was used for w, and measured values of b for each thermocouple were used.

Estimated uncertainties for the individual terms in Eq. (2) were used in the Taylor series method of uncertainty propagation to obtain the uncertainty in the heat-transfer coefficient as given below:

h	Uncertainty, Percent
10^{-4}	10
10^{-3}	7 .
10^{-2}	5

SECTION IV
RESULTS AND DISCUSSION

Windward centerline heat-transfer-rate distributions for Configuration UTN2 at a Reynolds number of 7.5 million are compared with calculated laminar, transitional, and turbulent values in Fig. 5. Descriptions of the calculation methods are given in Appendixes II and III. The beginning of boundary-layer transition was chosen as the point where the heating rate deviated from the laminar distribution. The end of transition could not be so well defined and hence was estimated from the shape of the heating-rate distribution.

For the 20-deg angle-of-attack case (Fig. 5a), the laminar data ($x/L < 0.4$) agree with two-dimensional calculations, indicating that cross-flow has not developed. The beginning of transition appears at $x/L = 0.4$, which is at the end of the region of abrupt cross-sectional change, and the flow apparently is not fully turbulent at the end of the body.

The laminar data (x/L < 0.3) at 30-, 40-, and 50-deg angles of attack (Figs. 5b, c, and d) agree fairly well with laminar crossflow calculations. The beginning of transition has moved slightly upstream of the region of abrupt cross-sectional change (0.3 < x/L < 0.4) in the 40- and 50-deg cases. The transitional and turbulent data agree well with the calculated values except for the transitional data at 50-deg angle of attack, where a localized peak is seen at an x/L value of 0.425.

To further investigate the unusual distribution at 50-deg angle of attack, a repeat run was made at 20 deg, and the results are shown in Fig. 6a. Significant differences in the data are seen at x/L values greater than or equal to 0.4. The most likely reason for these discrepancies is shown in Fig. 6b. Pretest and posttest lower surfaces are compared, showing that a wrinkle developed in the model skin during testing. Based on the data in Figs. 5 and 6, it is believed that this wrinkle developed between the 40- and the 50-deg runs (Figs. 5c and d, respectively). The skin wrinkled in a flat, unsupported region and may have done so because of thermal expansion.

Windward centerline heat-transfer-rate distributions for Configuration UTN2 at Reynolds numbers of 1.5 and 3.9 million are shown in Fig. 7. Two features of these data stand out. The beginning of boundary-layer transition is essentially fixed at x/L = 0.4 except at 20 deg angle of attack at the higher Reynolds number. The apparently laminar data at values of x/L greater than 0.4 at the lower Reynolds number are substantially above the calculated laminar values. This contrasts with the good agreement between data and calculations for transitional and turbulent boundary layers in the same region at the highest Reynolds number shown earlier in Fig. 5. The oil-flow photograph shown in Fig. 8 suggests two reasons for these results. The first is downstream influence of the complex flow field between x/L values of 0.3 and 0.4, which may be a function of Reynolds number and boundary-layer state. The second is flow divergence in the region under consideration. The assumption of zero flow divergence for the calculated values in this region was based on results from isolated delta wings with larger sweep angles than those of the present case and hence may not be correct. Flow divergence increases laminar heating substantially more than it does turbulent heating (Ref. 3).

Windward centerline heat-transfer-rate distributions for Configuration UTN7 at a Reynolds number of 7.5 million are shown in Fig. 9. Comparisons of the heating rates with calculated laminar values at x/L less than 0.25 are similar to those of Fig. 5 for Configuration UTN2. However, heating rates in the region of abrupt cross-sectional change (0.3 < x/L < 0.4) tend to be higher than the computed distributions, particularly at a = 20 deg. The transitional and turbulent heating rates and the calculated distributions are in good agreement except in the transition region at a = 50 deg, where the transitional data rise more quickly. Transition begins further downstream for this configuration but is completed in a shorter distance.

Windward centerline heat-transfer-rate distributions for Configuration UTN7 at Reynolds numbers of 1.5 and 3.9 million are shown in Fig. 10. With the exception of the 50-deg angle-of-attack case, agreement between data and calculated values at x/L values between 0.4 and 0.6 is closer than in the UTN2 case (Fig. 7).

Oil-flow photographs of Configuration UTN7 are shown in Fig. 11. Comparison of Fig. 11b with Fig. 8 indicates considerable difference in the flow pattern in the region of abrupt cross-sectional change (0.3 < x/L < 0.4).

Because of the significant differences in flow field in the region between x/L values of 0.3 and 0.6 between the two configurations, it is not clear what effect nose shape per se had on the beginning of transition. Only in two cases (Configuration UTN2, with $Re_{\infty,L}$ = 7.5 x 10⁶, a = 40 and 50 deg) did transition begin upstream of this region.

A comparison of the present results for the beginning of boundary-layer transition with the McDonnell Douglas Phase B transition correlation (Ref. 4) and VKF Phase B results (Refs. 5 and 6) is shown in Fig. 12.

Comparison of the present results for the extent of the transition zone with the correlation of Dhawan and Narasimha (Ref. 7) is shown in Fig. 13. Results for Configuration UTN7 are in general agreement with the correlation, whereas results for Configuration UTN2 are 50 percent higher.

Leeward centerline heat-transfer distributions at 7.5 million Reynolds number are shown in Fig. 14. Overall levels are approximately the same for the two configurations, with the details of the distributions being slightly different. Canopy-front heating rates (x/L = 0.2) are very high (about 50 percent of the windward level), with Configuration UTN2 having slightly higher rates. More complete discussions of the present test results are given in References 8 and 9.

SECTION V
CONCLUDING REMARKS

Heat-transfer tests were conducted on two space shuttle configurations at Mach number 8 to investigate the effects of nose geometry on windward and leeward heating and boundary-layer transition. Windward centerline heating on the noses (x/L < 0.3) of both configurations agreed with crossflow calculations for angles of attack of 30 deg and greater. Transitional and turbulent heating on the aft portion of the two configurations (x/L > 0.4) also agreed with the present calculation methods. Laminar heating on the aft portion of the configurations appeared to be significantly affected by the abrupt change in cross section as the nose merged into the aft fuselage and wing. Differences in the location of the beginning of transition and the length of transition zone were apparent for the two configurations; however, it was not clear whether these differences were attributable to the differences in nose shapes per se or to the abrupt cross-sectional changes. Overall leeward centerline heating levels were approximately the same for both configurations.

REFERENCES

1. Sivells, J. C. "Aerodynamic Design and Calibration of the VKF 50-Inch Hypersonic Wind Tunnels." AEDC-TDR-62-230 (AD299774), March 1963.

2. Touloukian, Y. S. and Buyco, E. H. Thermophysical Properties of Matter, Vol. 4, Specific Heat: Metallic Elements and Alloys. New York: IFI/Plenum, 1970.

3. Guard, F. L. and Schultz, H. D. "Space Shuttle Aerodynamic Heating Considerations." ASME Paper No. 70-HT/SpT-16, presented at the Space Technology and Heat Transfer Conference, Los Angeles, California, June 21-24, 1970.

4. Kipp, H. W. and Masek, R. V. "Aerodynamic Heating Constraints on Space Shuttle Vehicle Design." ASME Paper No. 70-HT/SpT-45, presented at the Space Technology and Heat Transfer Conference, Los Angeles, California, June 21-24, 1970.

5. Matthews, R. K., Eaves, R. H., Jr., and Martindale, W. R. "Heat-Transfer and Flow-Field Tests of the McDonnell-Douglas Martin Marietta Space Shuttle Configurations." AEDC-TR- (To be published).

6. Martindale, W. R., Matthews, R. K., and Trimmer, L. L. "Heat-Transfer and Flow-Field Tests of the General Dynamics Convair - North American Rockwell Space Shuttle Configurations." AEDC-TR-72-169 (AD755354), January 1973.

7. Dhawan, S. and Narasimha, R. "Some Properties of Boundary-Layer Flow During Transition from Laminar to Turbulent Motion." J. Fluid Mech., Vol. 3, Part 4 (April 1958), pp. 418-436.

8. Bertin, John J., Martindale, W. R., Faria, H. Tom, et al. "The Effect of Nose Geometry on the Aerothermodynamic Environment of Shuttle Entry Configurations." Aerospace Engineering Report 73001, The University of Texas at Austin, January 1973.

9. Bertin, John J., Faria, H. Tom, Goodrich, Winston D., and Martindale, W. R. "Effect of Nose Geometry on the Aerothermodynamic Environment of Shuttle Entry Configurations." AIAA Paper No. 73-638, presented at the AIAA 6th Fluid and Plasma Dynamic Conference, Palm Springs, California, July 16-18, 1973.

10. Rasmussen, M. L. "On Hypersonic Flow Past an Unyawed Cone." AIAA J., Vol. 5, No. 8 (August 1967), pp. 1495-1497.

11. Stallings, Robert L., Jr. "Experimentally Determined Local Flow Properties and Drag Coefficients for a Family of Blunt Bodies at Mach Numbers from 2.49 to 4.63." NASA TR R-274, October 1967.

12. Moretti, Gino. "Inviscid Blunt Body Shock Layers." Pibal Report No. 68-15, June 1968.

13. Thomas, A. C. and Perlbachs, A. "Application of Ground Test Data to Reentry Vehicle Design." AFFDL-TR-66-229, January 1967.

14. Fehrman, A. L. and Masek, R. V. "Study of Uncertainties of Predicting Space Shuttle Thermal Environment." Report MDC E0639, June 1972.

15. Scottoline, C. A. "Determination of Aerothermodynamic Uncertainties with Application to Space Shuttle Vehicles," in Space Shuttle Aerothermodynamics Technology Conference, Volume II: Heating. NASA TM X-2507, February 1972, pp. 503-518.

16. Eckert, E. R. G. "Engineering Relations for Friction and Heat Transfer to Surfaces in High Velocity Flow." J. Aeron. Sci., Vol. 22, No. 8 (August 1955), pp. 585-587.

17. Spalding, D. B. and Chi, S. W. "The Drag of a Compressible Turbulent Boundary Layer on a Smooth Flat Plate with and without Heat Transfer." J. Fluid Mech., Vol. 18, Part 1 (January 1964), pp. 117-143.

18. Komar, James J. "Skin-Friction Predictions in Turbulent Compressible Flow." AIAA J., Vol. 4, No. 7 (July 1966), pp. 1307-1308.

19. Colburn, A. P. "A Method of Correlating Forced Convection Heat-Transfer Data and a Comparison with Fluid Friction." Trans. Amer. Inst. Chem. Eng., Vol. 29 (1933), pp. 174-210.

20. Vaglio-Laurin, Roberto. "Laminar Heat Transfer on Three Dimensional Blunt Nosed Bodies in Hypersonic Flow." ARS J., Vol. 29, No. 2 (February 1959), pp. 123-129.

21. Vaglio-Laurin, Roberto. "Turbulent Heat Transfer on Blunt-Nosed Bodies in Two-Dimensional and General Three-Dimensional Hypersonic Flow." J. Aero-Space Sci., Vol. 27, No. 1 (January 1960), pp. 27-36.

22. Adams, John C., Jr. and Martindale, William R. "Hypersonic Lifting Body Windward Surface Flow-Field Analysis for High Angles of Incidence." AEDC-TR-73-2, February 1973.

APPENDIXES
I. ILLUSTRATIONS
II. FLOW-FIELD METHODS
III. BOUNDARY-LAYER CALCULATION METHODS
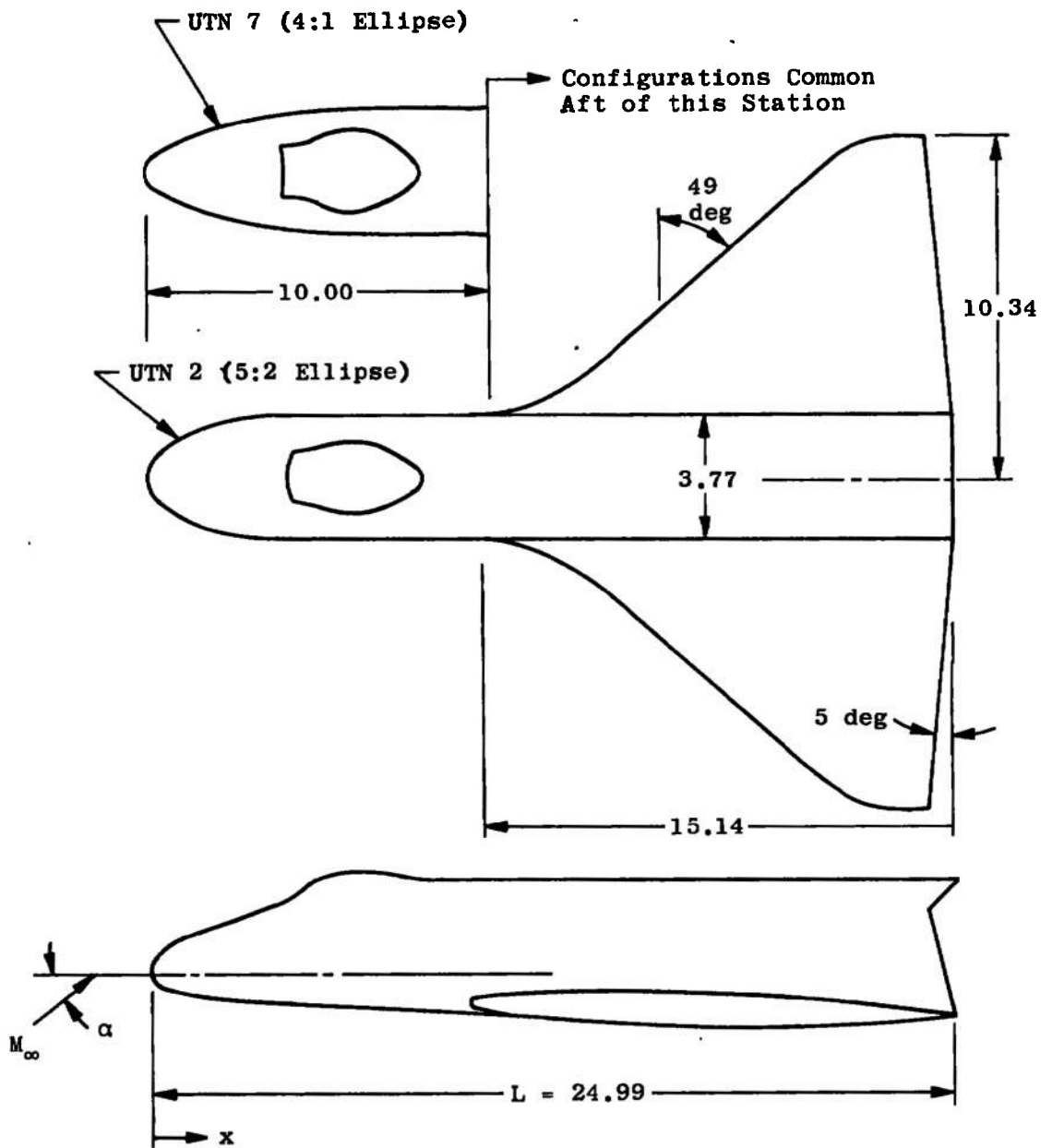
All Dimensions in Inches

Fig. 1 Model Drawing
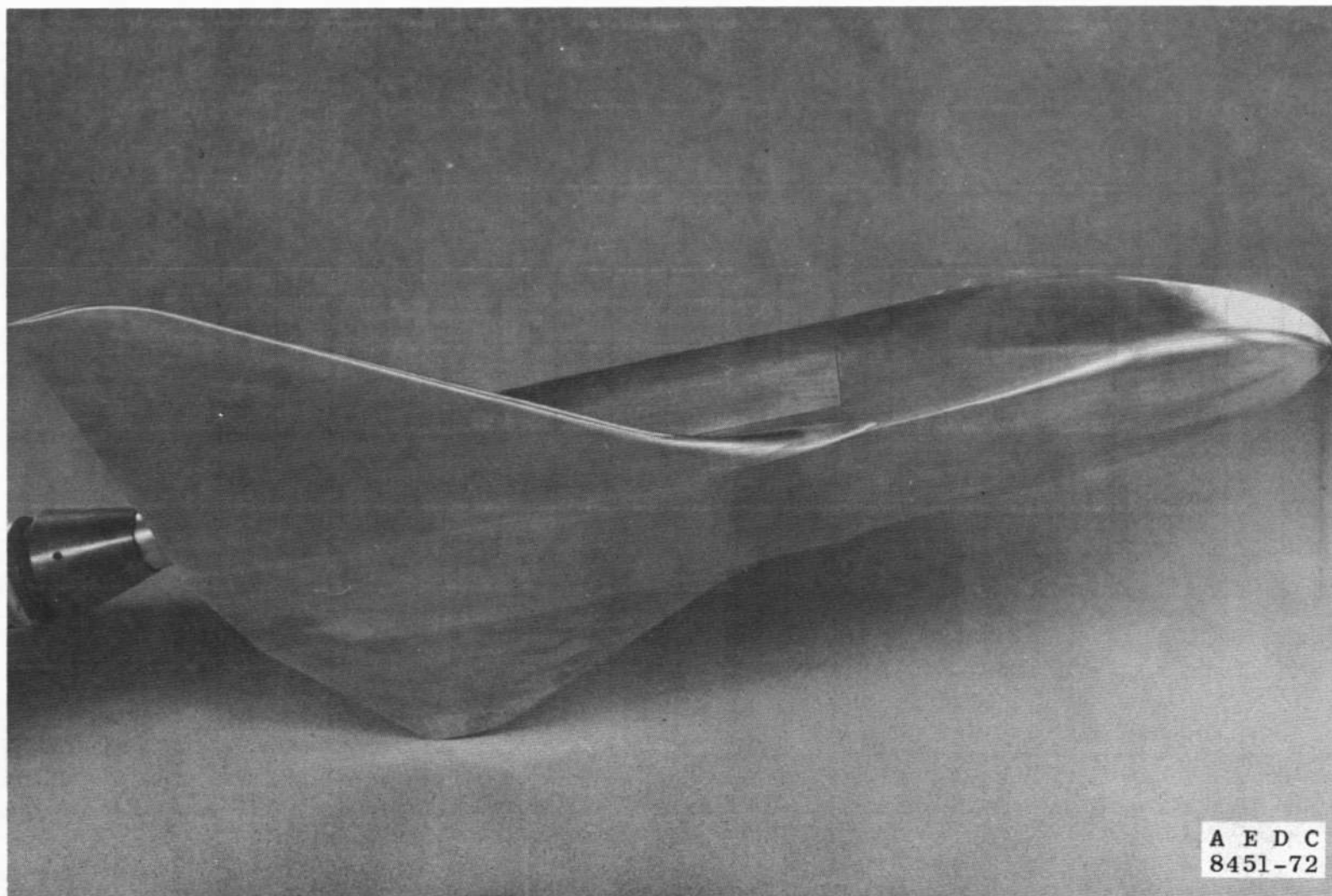
Fig. 2 Photograph of Configuration UTN2
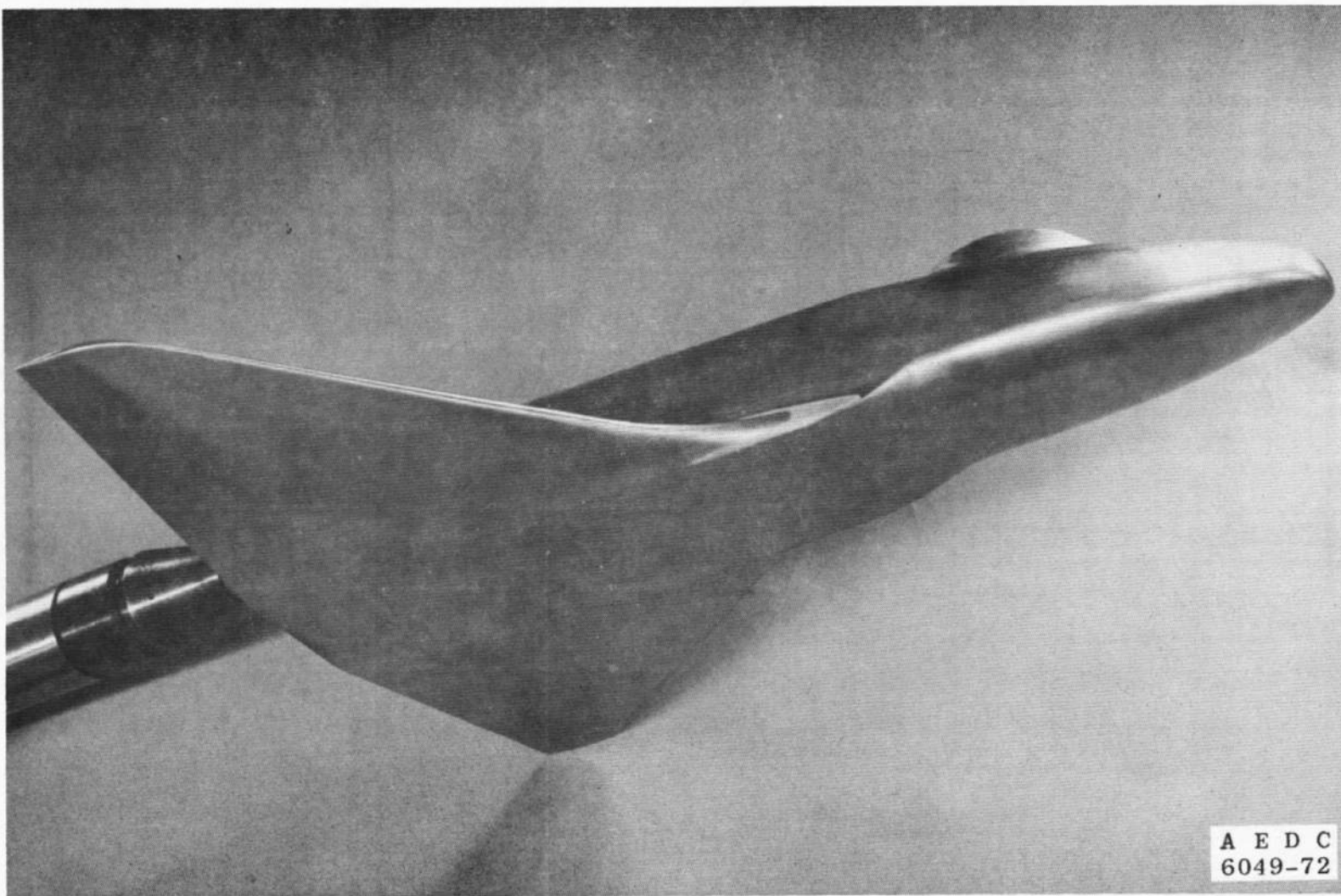
Fig. 3 Photograph of Configuration UTN7
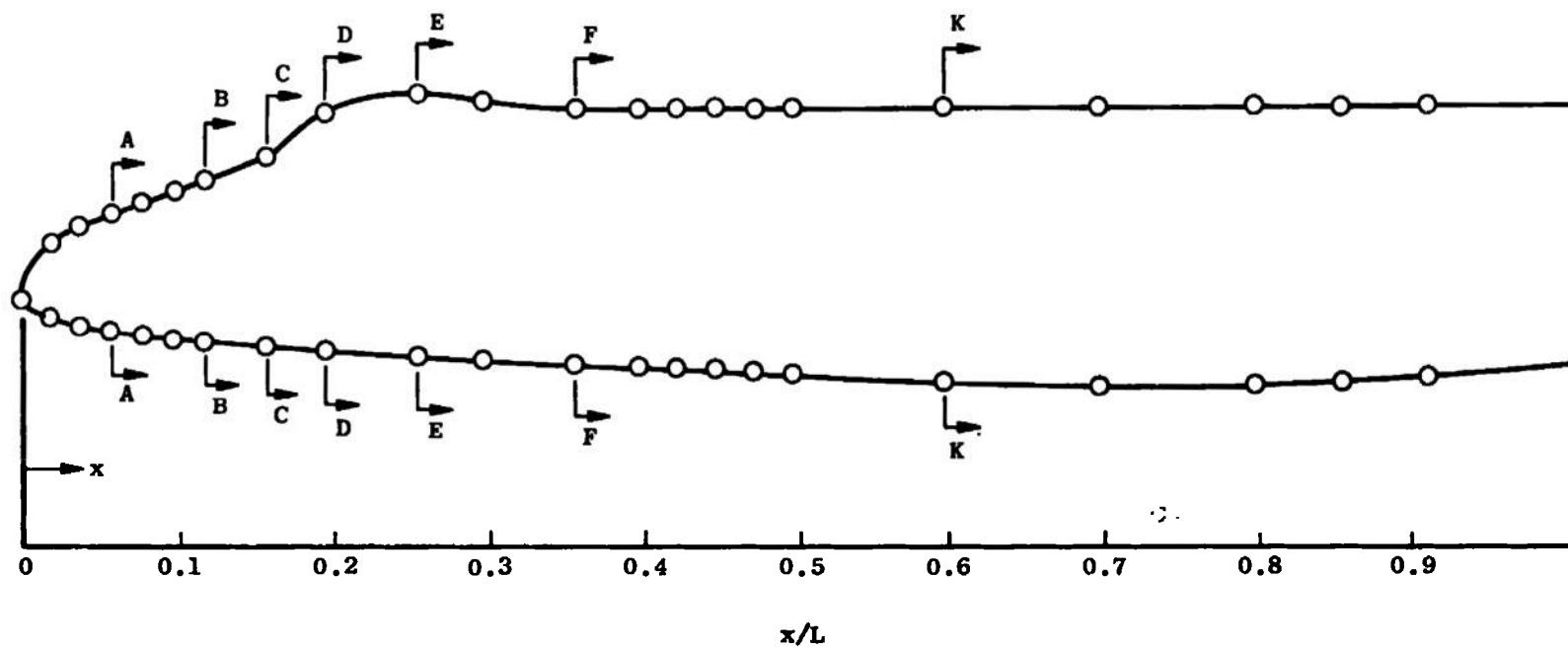
a. Windward and Leeward Centerlines
Fig. 4 Thermocouple Locations

Section AA
x/L = 0.06

Section BB
x/L = 0.12

Section CC
x/L = 0.16

Section DD
x/L = 0.20

Section EE
x/L = 0.26
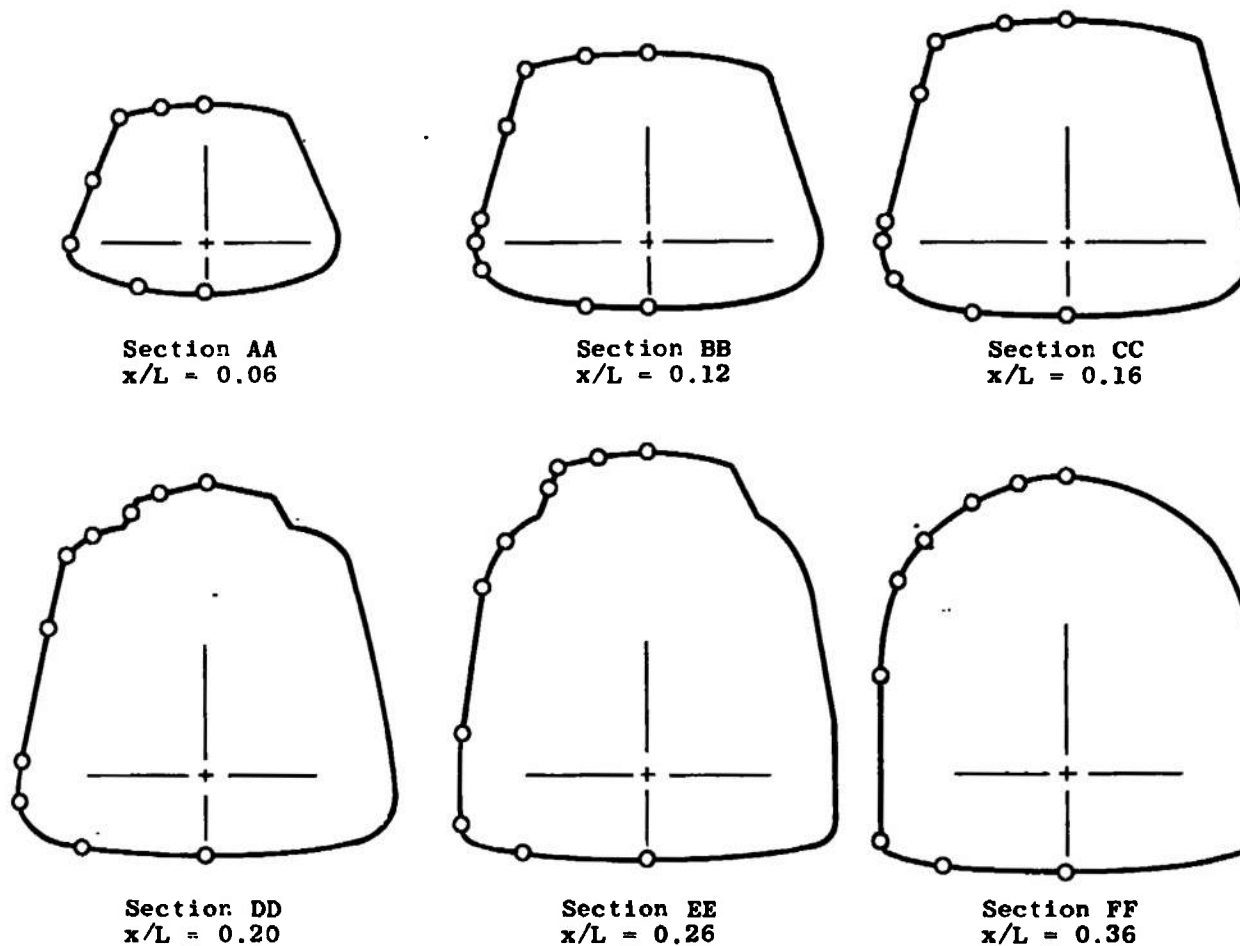
Section FF
x/L = 0.36

b. Cross Sections for Configuration UTN2
Fig. 4 Continued

Section AA
x/L = 0.06

Section BB
x/L = 0.12

Section CC
x/L = 0.16

Section DD
x/L = 0.20

Section EE
x/L = 0.26

Section FF
x/L = 0.36
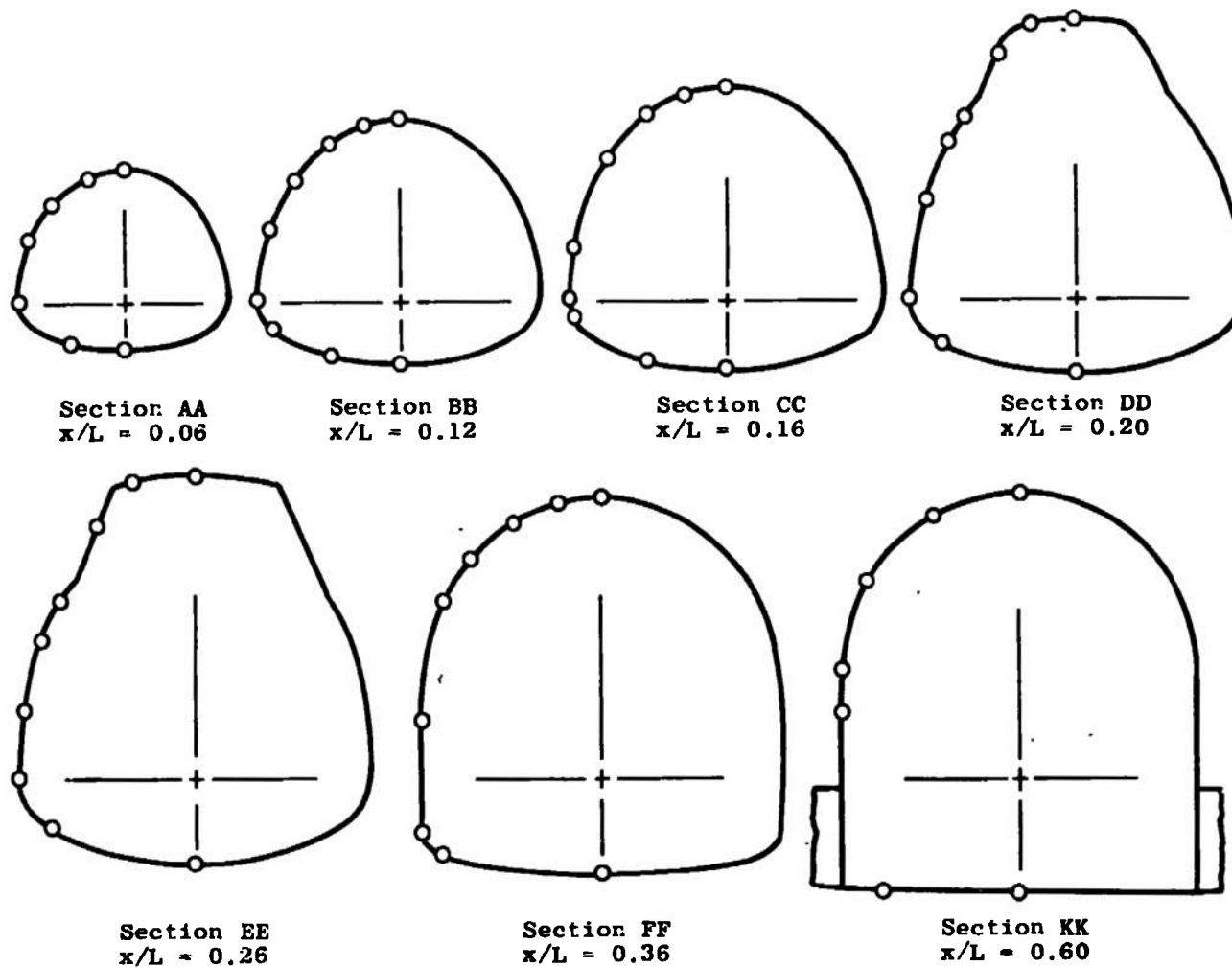
Section KK
x/L = 0.60

c. Cross Sections for Configuration UTN7
Fig. 4 Concluded
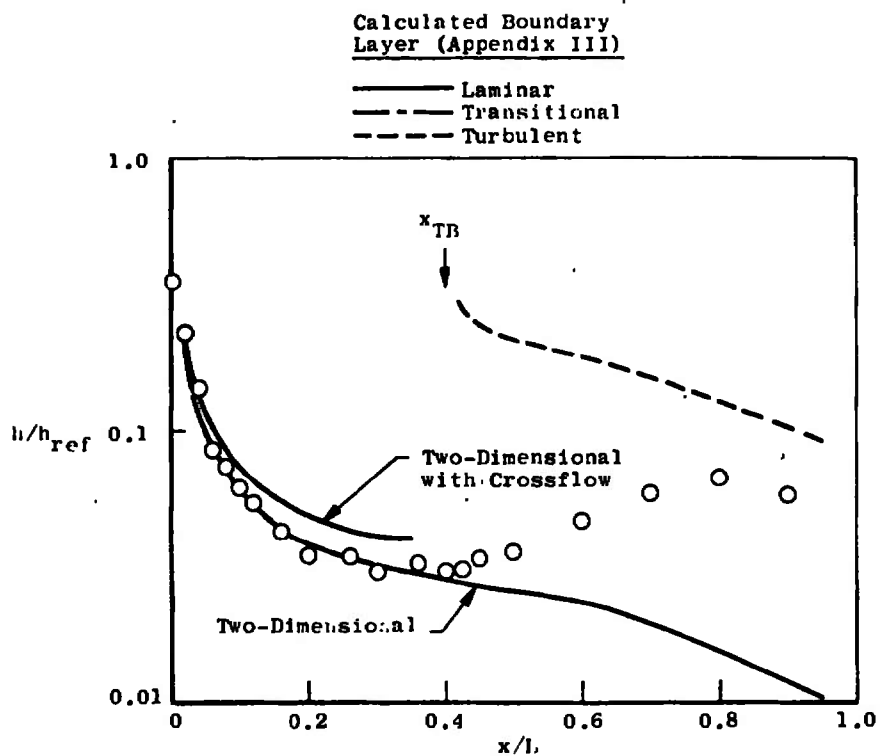
a. $a = 20$ deg
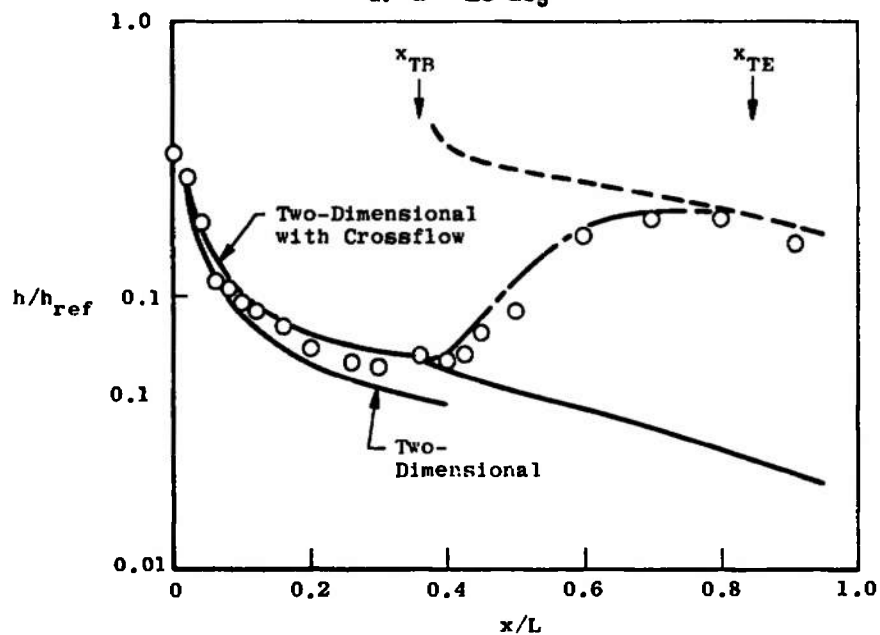
b. $a = 30$ deg

Fig. 5 Windward Centerline Heat-Transfer-Rate Distributions for
Configuration UTN2 at $Re_{\infty,L} = 7.5 \times 10^6$

c. a = 40 deg

d. a = 50 deg
Fig. 5 Concluded

18

a. Comparison of Heat-Transfer Rates for Original and
Repeat Runs at a = 20 deg
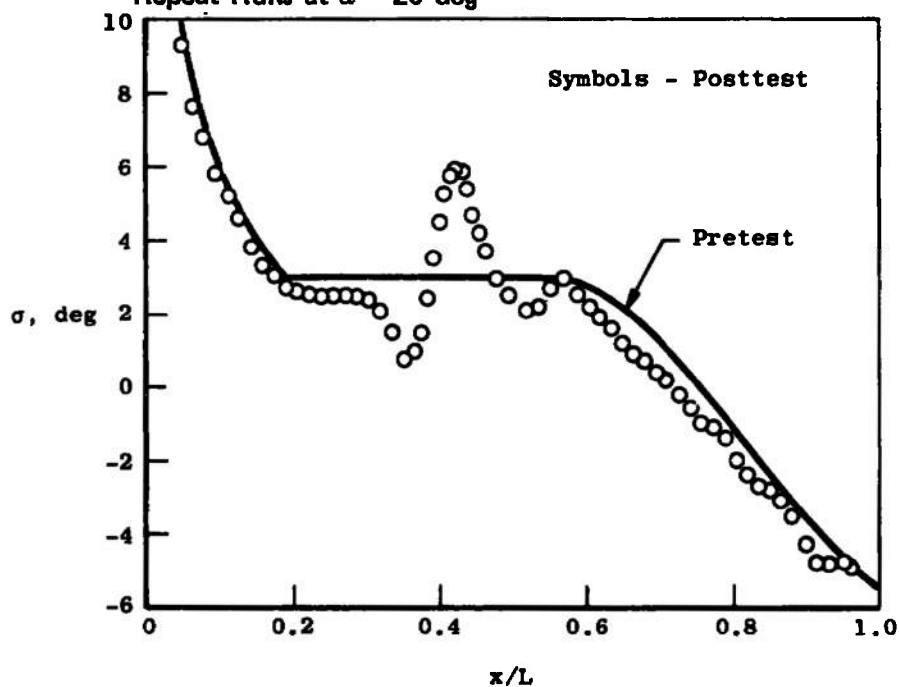
b. Comparison of Pretest and Posttest Lower Surface Angles
for Configuration UTN2

Fig. 6 Comparisons of Original and Repeat Measurements of Windward
Centerline Heat-Transfer Rate and Surface Angle

a. a = 20 deg

b. a = 30 deg
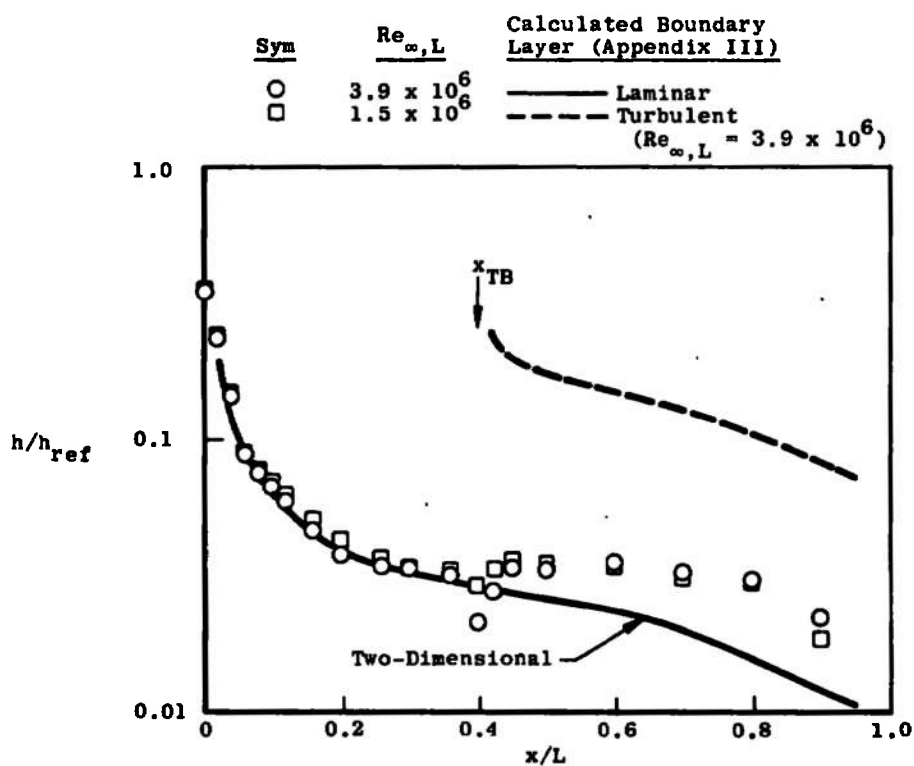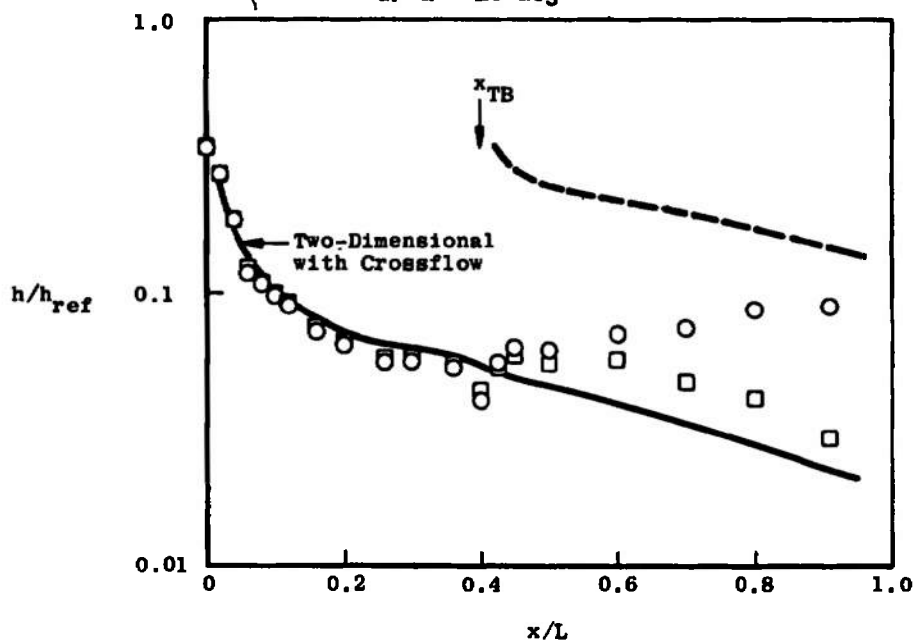
Fig. 7 Windward Centerline Heat-Transfer-Rate Distributions for Configuration UTN2 at $Re_{\infty,L}$ = 3.9 x 10⁶ and 1.5 x 10⁶

20

c. $a = 40$ deg

d. $a = 50$ deg
Fig. 7 Concluded

Fig. 8 Oil-Flow Photograph of Configuration UTN2 at a = 35 deg and $Re_{\infty, L}$ = 1.5 x 10^6

a. a = 20 deg
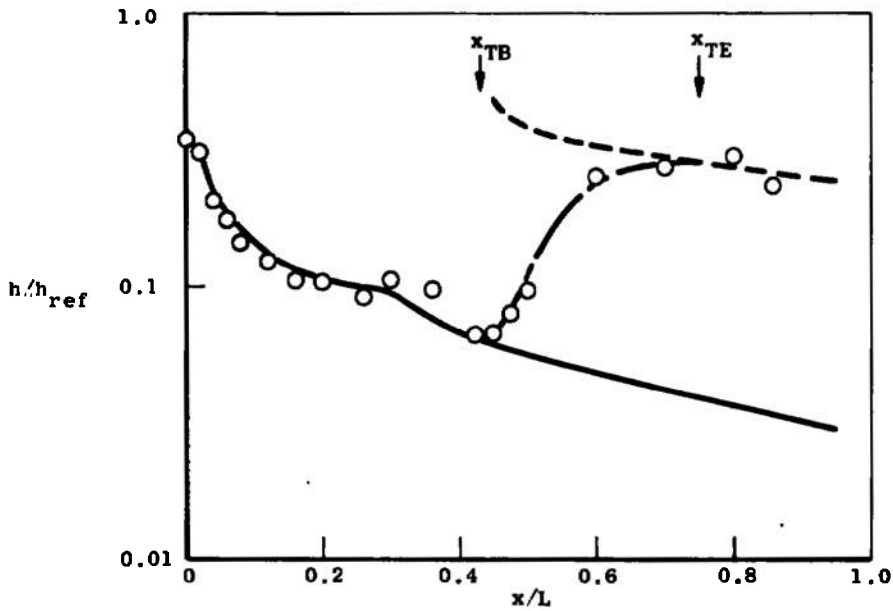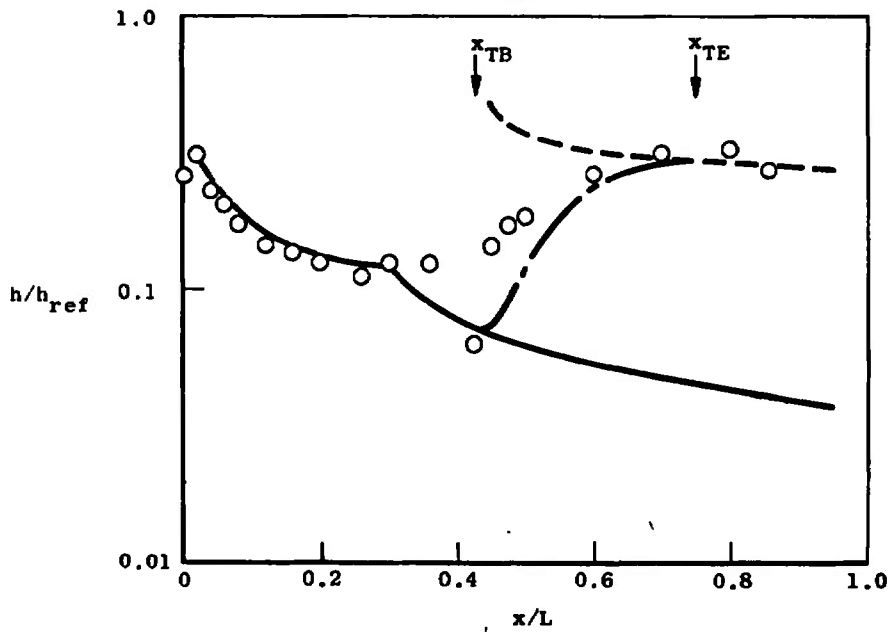
b. a = 30 deg

Fig. 9 Windward Centerline Heat-Transfer-Rate Distributions for
Configuration UTN7 at $Re_{\infty,L}$ = 7.5 x 10^6

Calculated Boundary
Layer (Appendix III)
————— Laminar (Two-Dimensional
with Crossflow)
—·—·— Transitional
— — — Turbulent

c. $a = 40$ deg

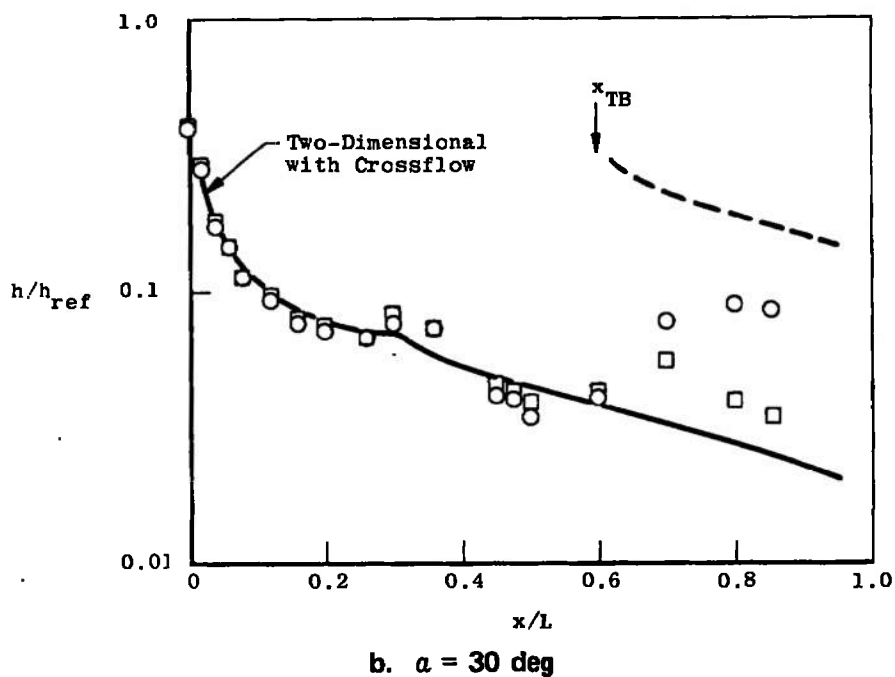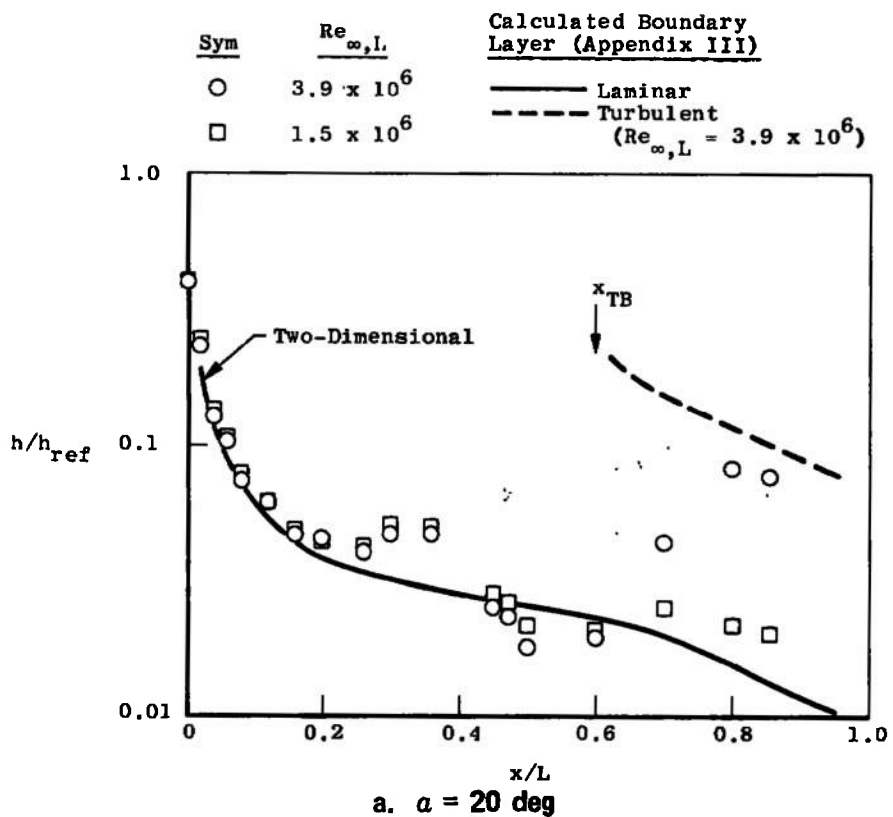d. $a = 50$ deg
Fig. 9 Concluded

a. a = 20 deg

b. a = 30 deg

Fig. 10 Windward Centerline Heat-Transfer-Rate Distributions for Configuration UTN7 at $Re_{\infty,L}$ = 3.9 x 10⁶ and 1.5 x 10⁶

c. $a = 40$ deg
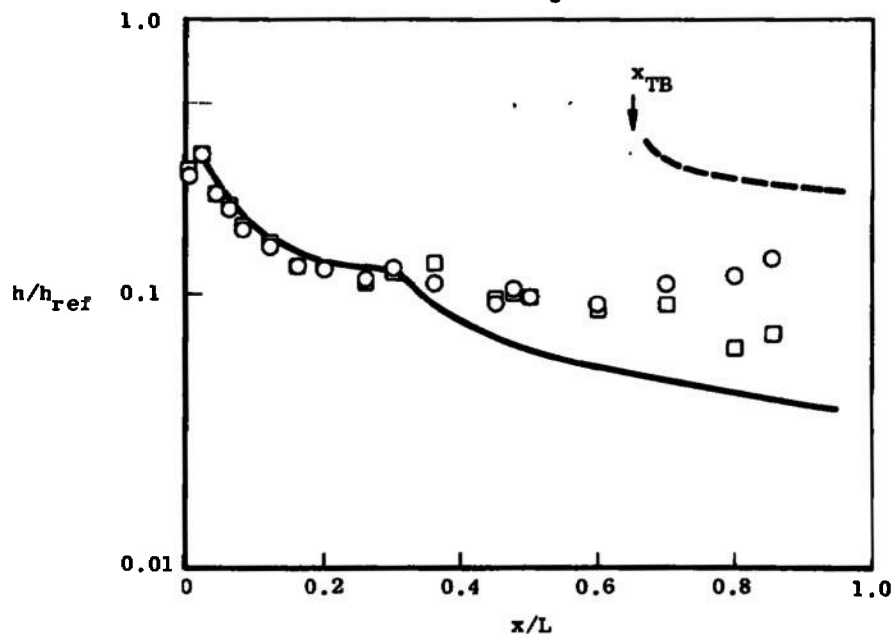

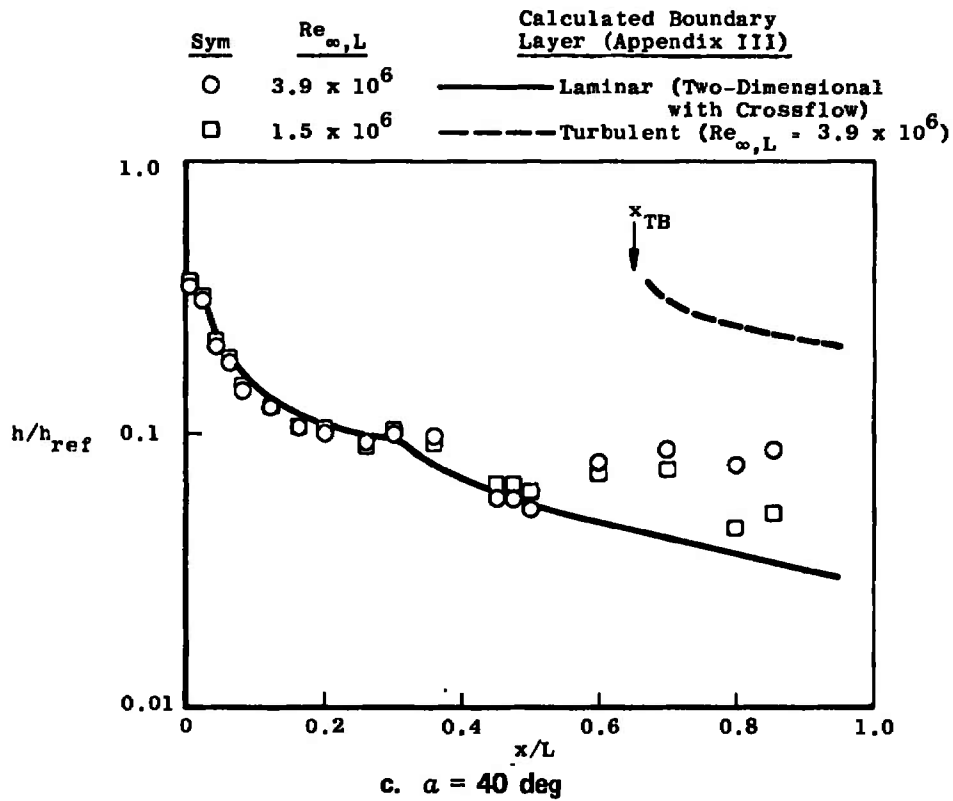d. $a = 50$ deg
Fig. 10 Concluded

x/L

0   0.1   0.2   0.3   0.4   0.5   0.6   0.7   0.8   0.9   1.0
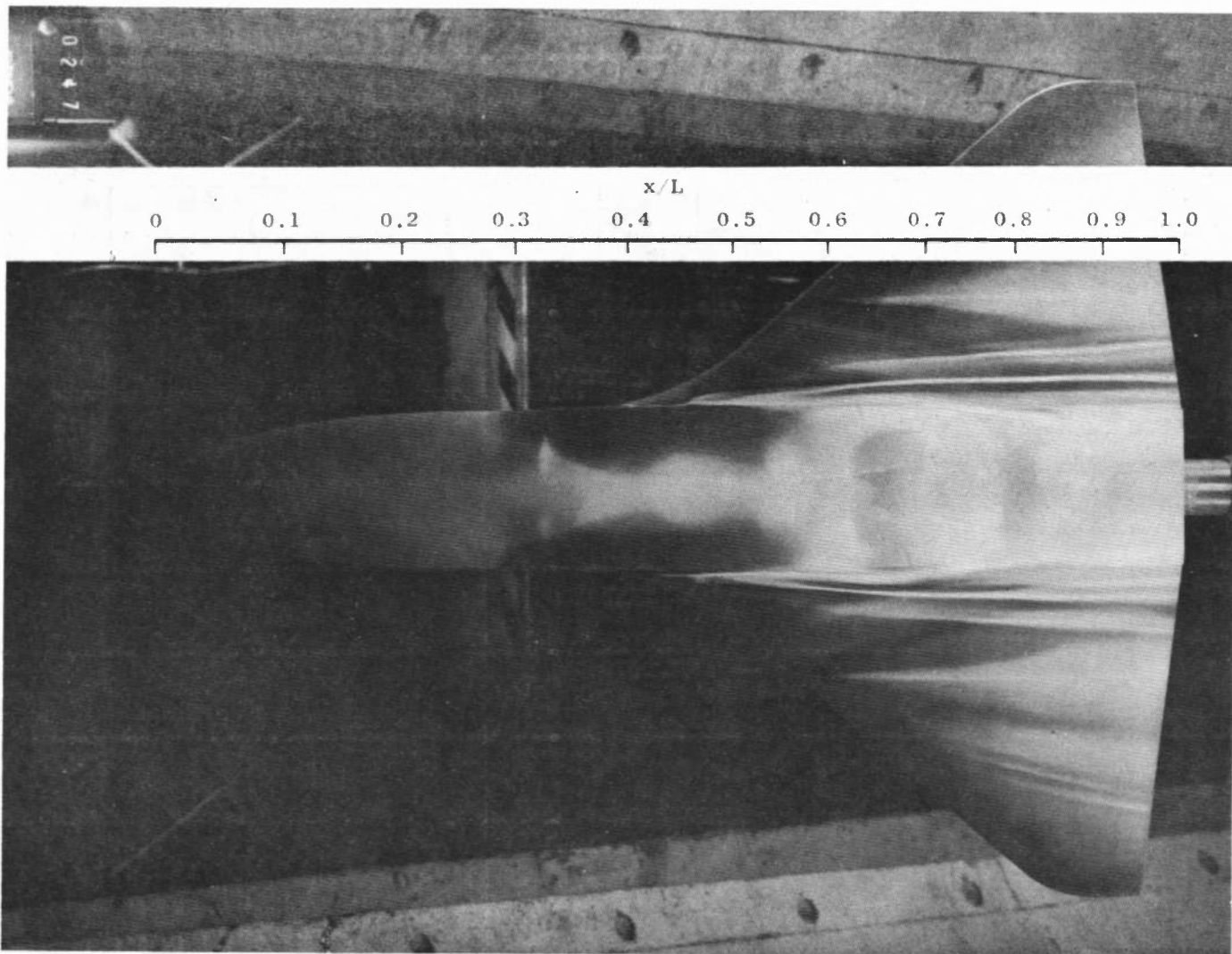
a. a = 20 deg
Fig. 11 Oil-Flow Photographs of Configuration UTN7 at $Re_{\infty,L}$ = 1.5 x 10^6
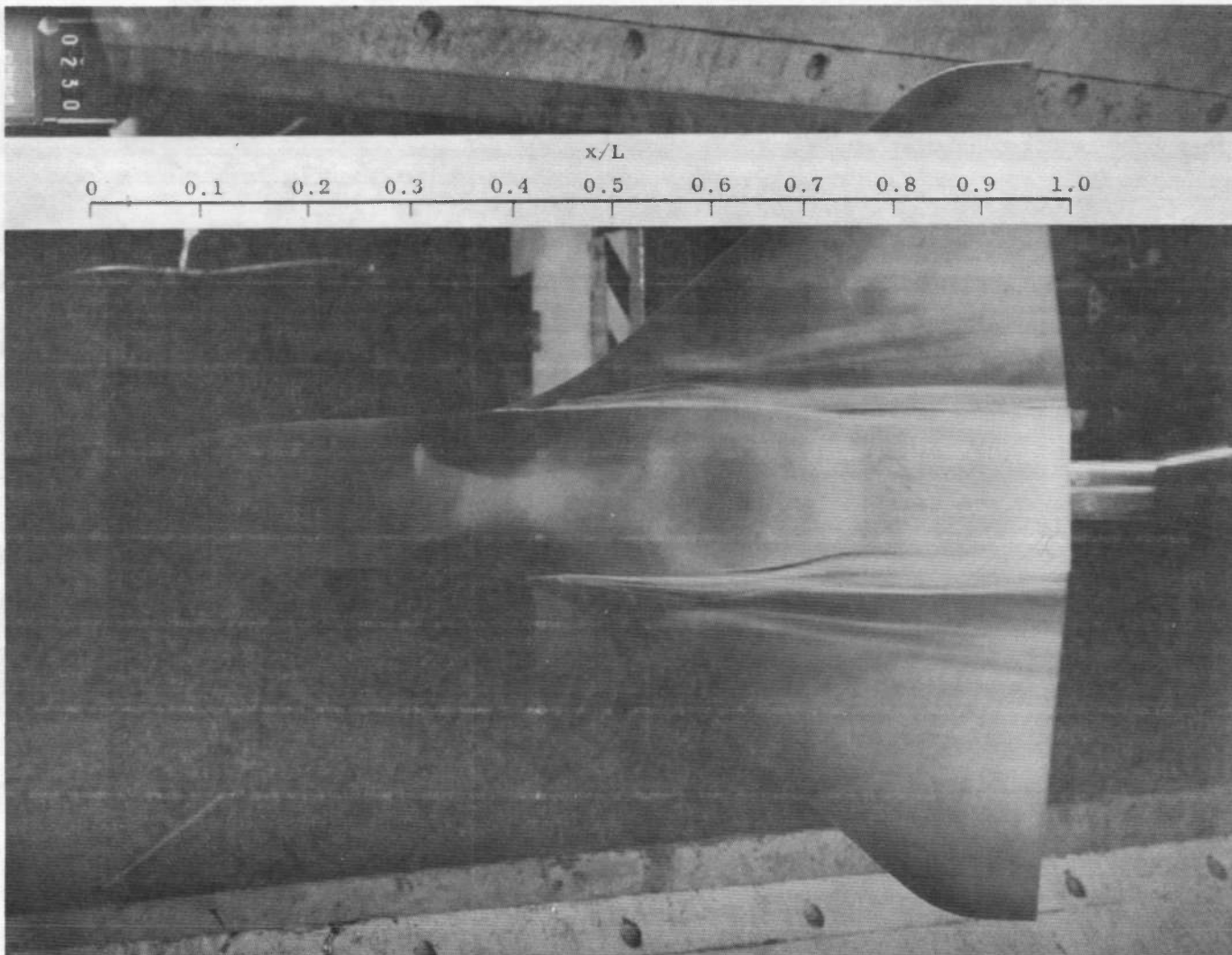
b. a = 35 deg
Fig. 11 Concluded

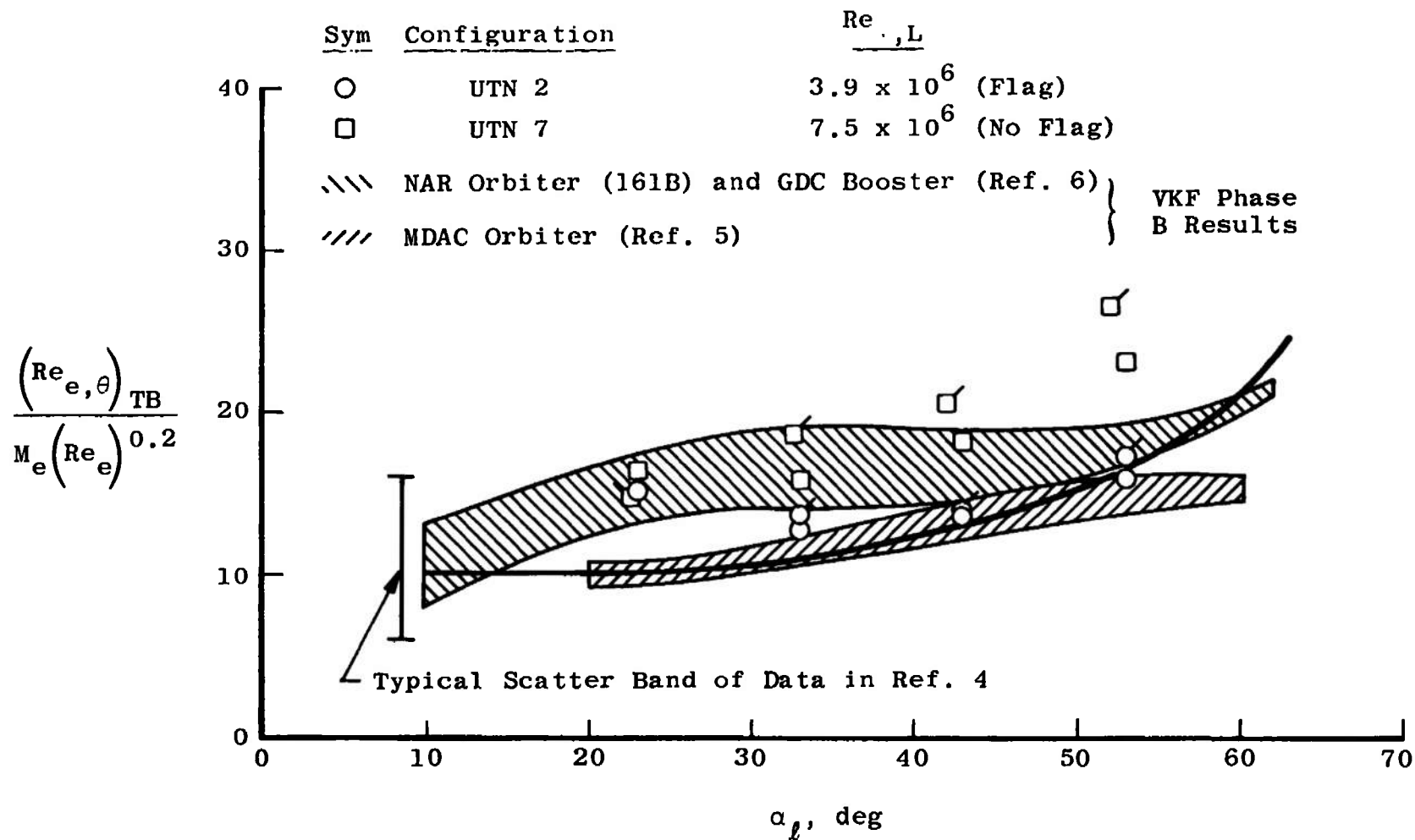Fig. 12 Comparison of Present Transition Results with the McDonnell Douglas Phase B Transition
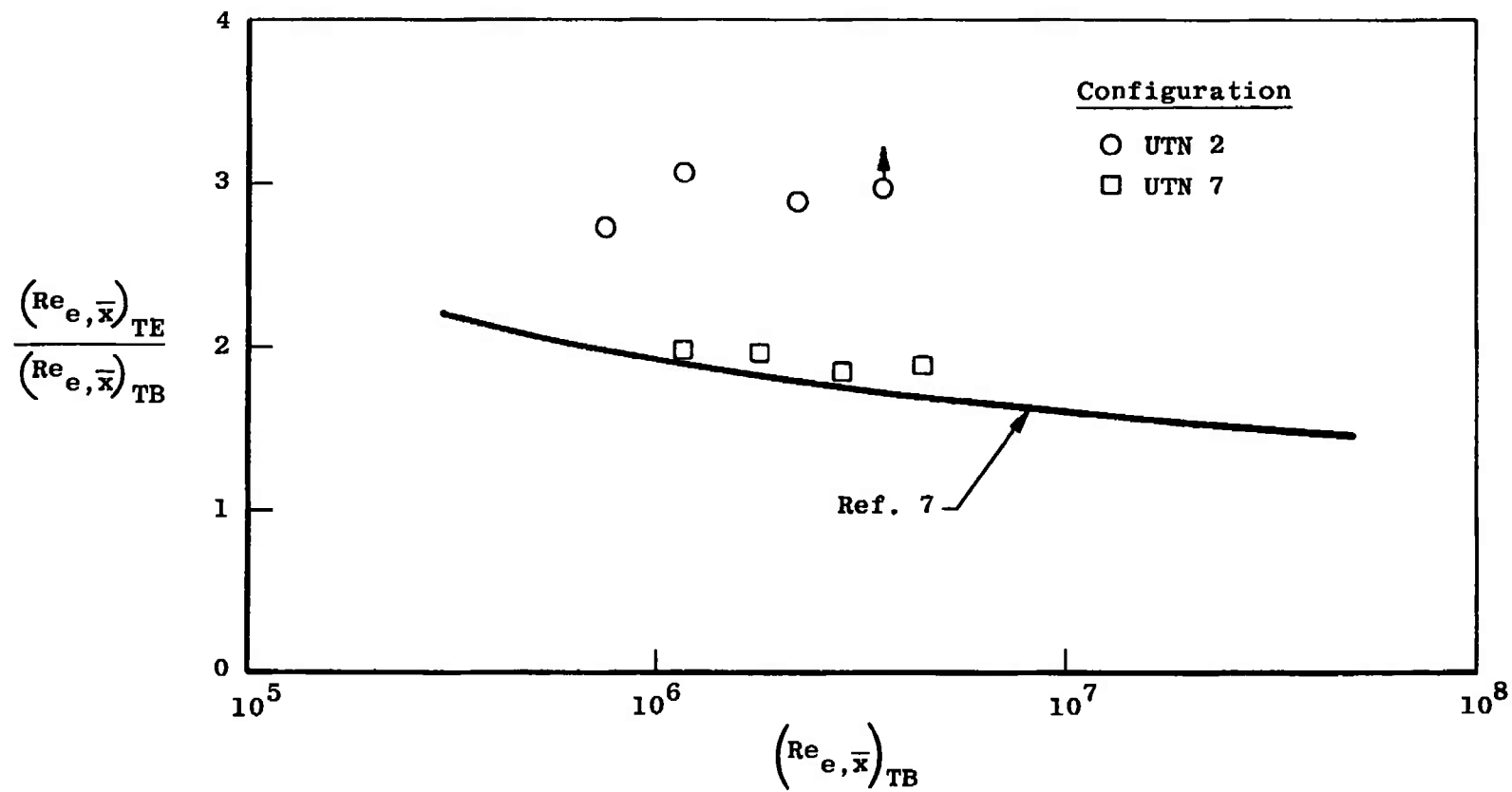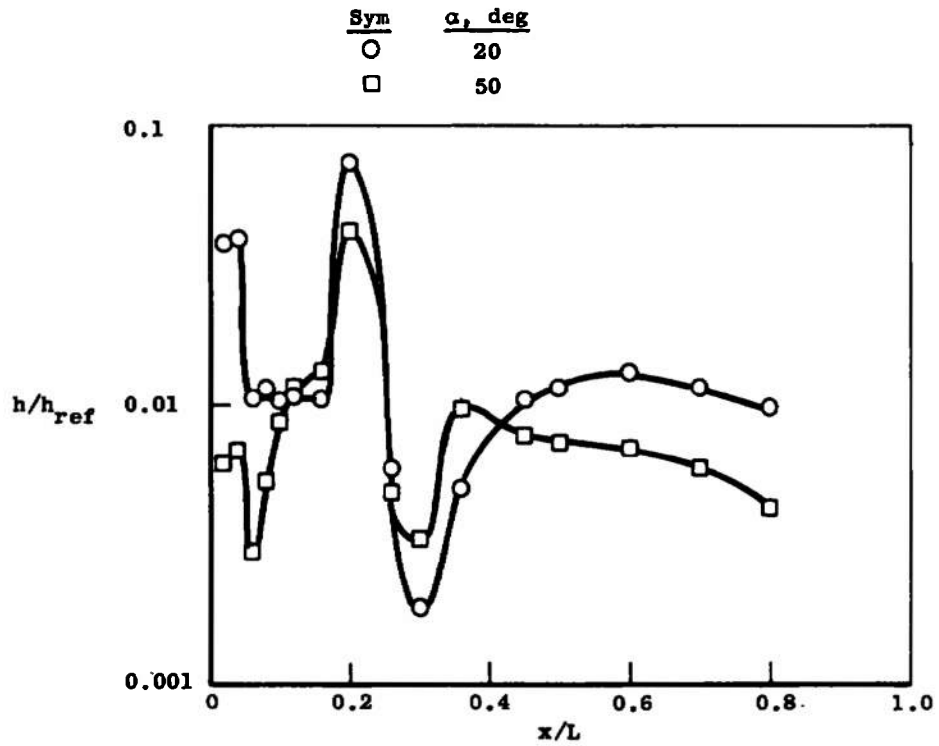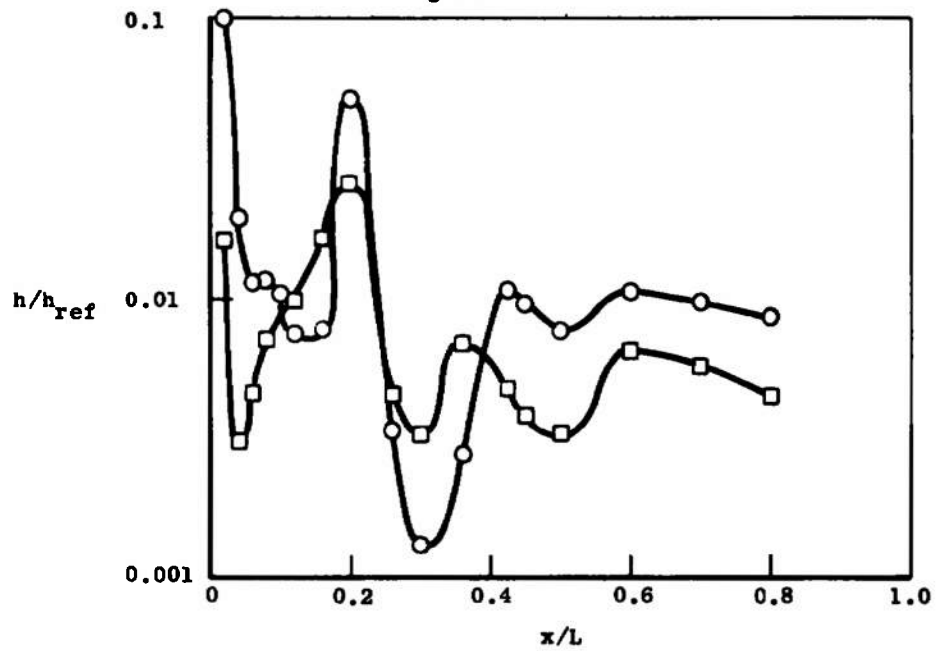Correlation Parameter and VKF Phase B Data

Fig. 13 Comparison of the Present Results for the Extent of the Transition Zone with the Correlation of Dhawan and Narasimha

a. Configuration UTN2

b. Configuration UTN7
Fig. 14 Leeward Centerline Heat-Transfer-Rate Distributions at
$Re_{\infty,L} = 7.5 \times 10^6$

APPENDIX II
FLOW-FIELD METHODS

Model shock angles measured from shadowgraph photographs are compared with tangent wedge, tangent cone, and parallel shock values in Fig. II-1. Though there is considerable scatter in the measurements as plotted, the tangent cone values are seen to best represent the results. The tangent cone values shown in Fig. II-1 were computed using the following equation from Ref. 10:

$$\frac{\sin \theta_s}{\sin \alpha_\ell} = \left[\frac{\gamma + 1}{2} + \frac{1}{(M_\infty \sin \alpha_\ell)^2} \right]^{\frac{1}{2}}$$

(II-2)

Centerline surface pressure measurements on Phase B Space Shuttle models indicate that surface pressures are generally between tangent cone and modified Newtonian theory. Examples of these data for the McDonnell Douglas Phase B orbiter, taken from Ref. 5, are shown in Fig. II-2. Modified Newtonian theory was used in the present calculations. With both shock angle and surface pressure calculated, all other properties at the boundary-layer edge were determined by crossing the shock using the oblique shock relations followed by an isentropic compression to surface pressure.

Nose cross sections of Configuration UTN2 were approximated by double-radius blunt bodies and the crossflow velocity gradient obtained from Fig. 20 of Ref. 11. The crossflow velocity gradient for the elliptical cross sections of Configuration UTN7 was obtained by using the shock standoff distances of Ref. 12 and Eq. (B-2) from Ref. 11. These crossflow velocity gradients were then applied over the following regions in the boundary-layer calculations, based on the oil-flow photographs.

Configuration	Crossflow Region
UTN2	$0 < x/L \leqslant 0.36$
UTN7	$0 < x/L \leqslant 0.30$

Results obtained from the delta wing flow-field correlations of Ref. 13 indicate that true crossflow is not achieved on a 49-deg sweep delta wing at angles of attack of 50 deg or less. Furthermore, it was shown in Ref. 3 that streamline divergence effects are significant on delta wing centerline heating only at values of angle of attack significantly greater than the apex angle or, in the case of the present wing, 41 deg. For these reasons no crossflow or streamline divergence was applied to the centerline boundary-layer calculations in the aft region.
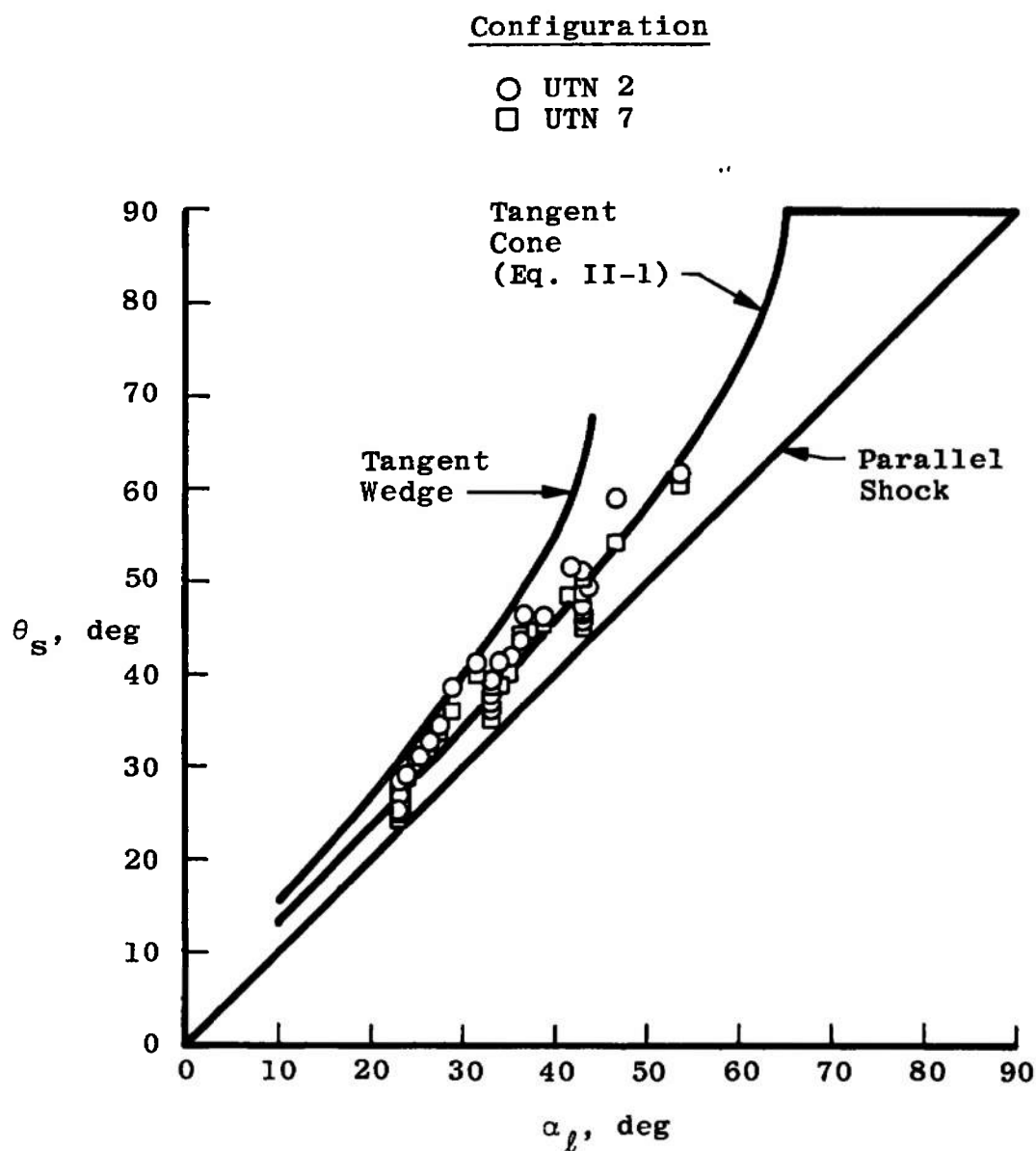
Fig. II-1 Comparison of Shock-Angle Measurement with Analytical Calculations

Sym	α, deg
O	10
□	20
△	30
◇	40
▽	50
D	60

————— Tangent Cone

— — — — Modified Newtonian

$M_\infty = 8$

$Re_{\infty,L} = 6.6 \times 10^6$

$M_\infty \approx 10.5$

$Re_{\infty,L} \approx 10^7$

α, deg

α, deg

Fig. II-2 MDAC Orbiter - Windward Centerline Pressure Distributions

APPENDIX III
BOUNDARY-LAYER CALCULATION METHODS

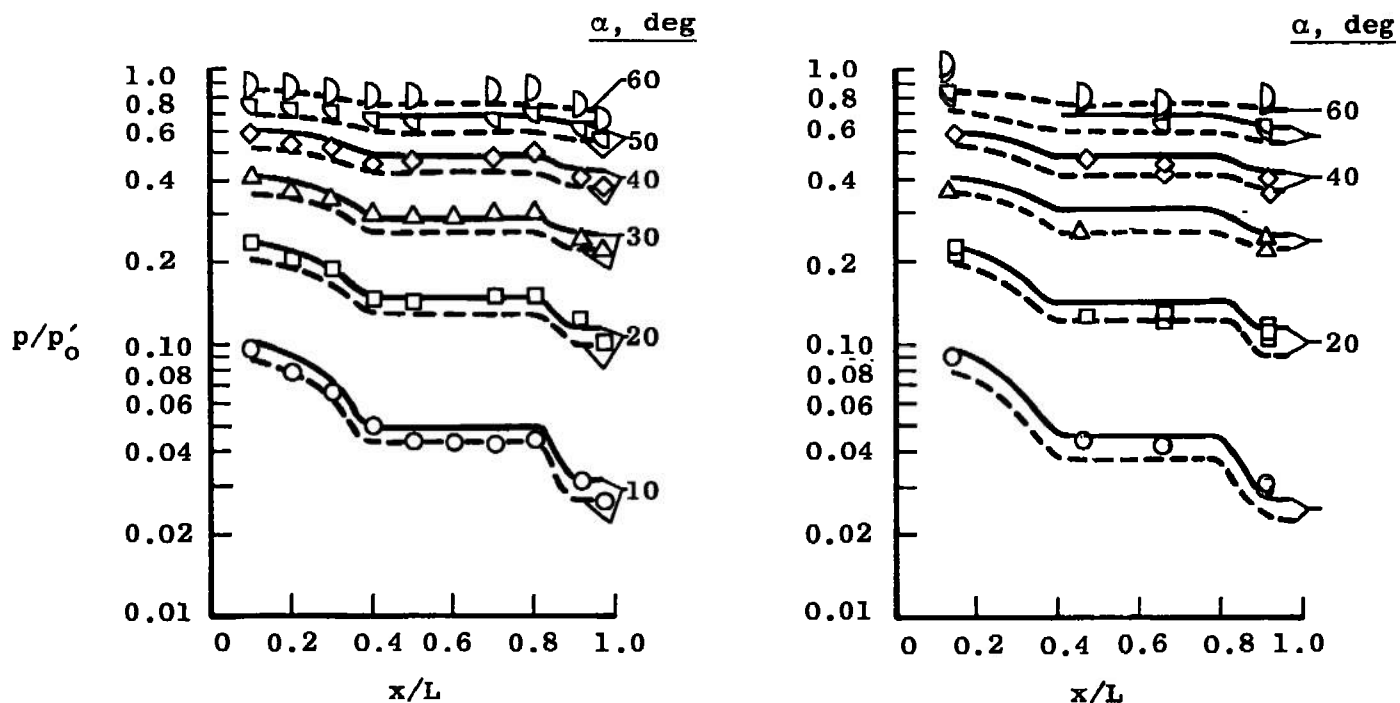The boundary-layer calculations in the present report use the basic methods which have become typical in data comparisons by Space Shuttle contractors (see Refs. 14 and 15). These are the Eckert Reference Enthalpy method (Ref. 16) for laminar flow and the Spalding-Chi method (Refs. 17, 18, and 19) for turbulent flow. Crossflow corrections for nose region were obtained using the crossflow velocity gradients as outlined in Appendix II and equations for equivalent surface distances from Refs. 20 and 21. Transitional heating rates were calculated using the laminar and turbulent rates and Eq. (11) of Ref. 7.

A comparison of present results for heat-transfer rates and momentum thickness Reynolds number with those obtained using a nonsimilar numerical calculation (Ref. 22) and the same edge conditions is shown in Fig. III-1. The heating-rate comparison is good, but a significant difference between the methods occurs in the momentum thickness Reynolds number at the rear of the body.
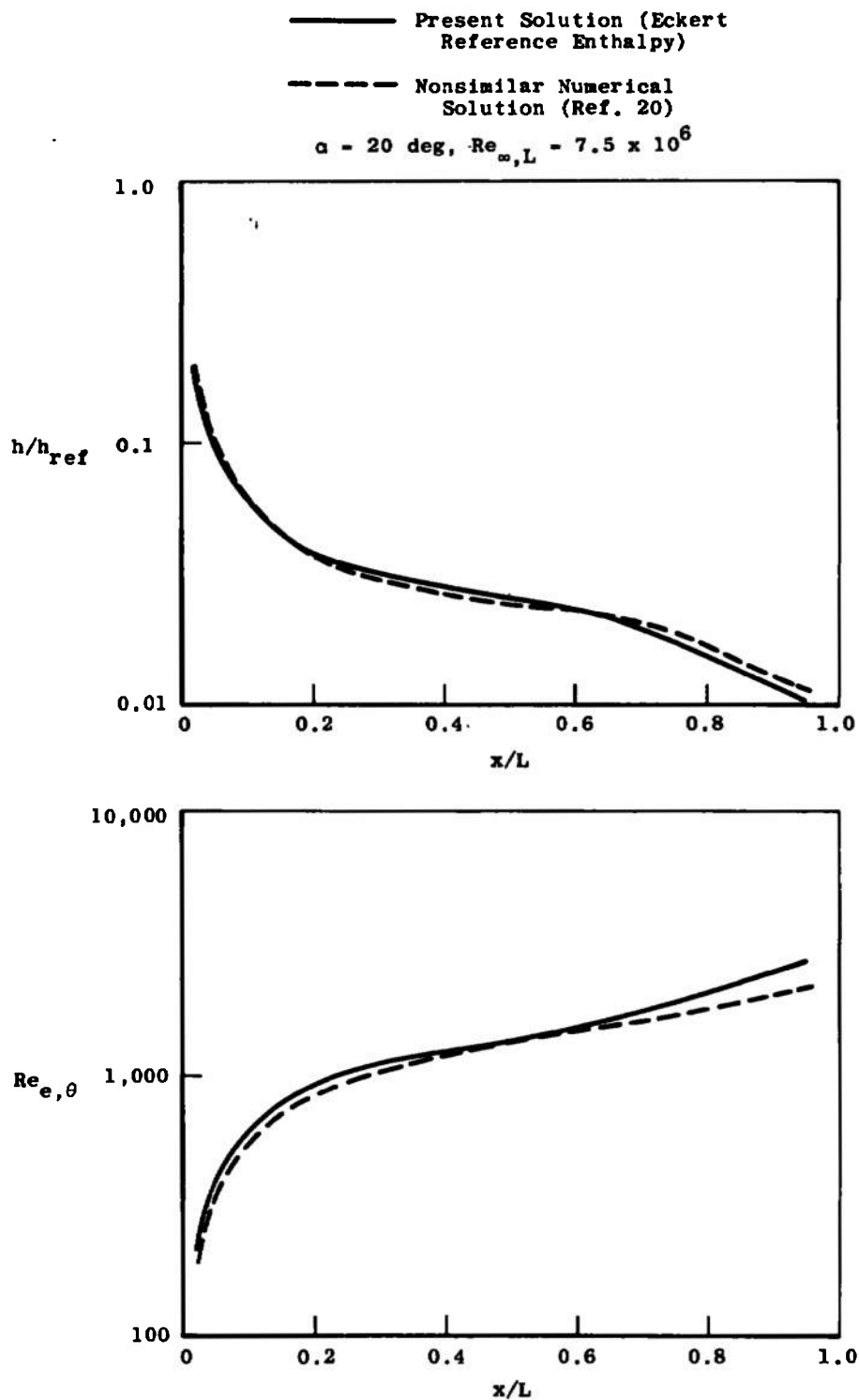
Fig. III-1 Comparison of Present Solution and a Nonsimilar Numerical Solution for Laminar Heat-Transfer Rates and $Re_{e,\theta}$

DOCUMENT CONTROL DATA - R & D

(Security classification of title, body of abstract and indexing annotation must be entered when the overall report is classified)

1 ORIGINATING ACTIVITY *(Corporate author)*	2a. REPORT SECURITY CLASSIFICATION
Arnold Engineering Development Center Arnold Air Force Station, Tennessee 37389	UNCLASSIFIED
	2b GROUP N/A

3 REPORT TITLE

HEAT-TRANSFER TESTS OF TWO SPACE SHUTTLE ORBITER CONFIGURATIONS AT MACH NUMBER 8

4 DESCRIPTIVE NOTES *(Type of report and inclusive dates)*

Final Report -- August 25 through September 28, 1972

5 AUTHOR(S) *(First name, middle initial, last name)*

W. R. Martindale, ARO, Inc.

6 REPORT DATE	7a TOTAL NO OF PAGES	7b. NO OF REFS
January 1974	44	22

8a CONTRACT OR GRANT NO	9a ORIGINATOR'S REPORT NUMBER(S)
b PROJECT NO	AEDC-TR-73-59
c Program Element 921E-1	9b OTHER REPORT NO(S) *(Any other numbers that may be assigned this report)*
d.	ARO-VKF-TR-72-198

10 DISTRIBUTION STATEMENT

Approved for public release; distribution unlimited.

11 SUPPLEMENTARY NOTES	12 SPONSORING MILITARY ACTIVITY
Available in DDC.	NASA - Manned Spacecraft Center SMD - Thermal Technical Branch Houston, TX 77958

13 ABSTRACT

Heat-transfer tests were conducted on two Space Shuttle configurations at Mach number 8 to investigate the effects of nose geometry on windward and leeward heating and boundary-layer transition. Free-stream Reynolds number based on model length was varied from 1.5 to 7.5 million at angles of attack from 20 to 50 deg. Windward centerline heating rates were in general agreement with calculated values except for laminar rates downstream of the wing/body junction. Differences in the location of the beginning of transition and the length of the transition zone were observed for the two configurations, but it was not clear whether variation in nose shape per se or the abrupt cross-sectional change from the nose to the aft fuselage and wing was the controlling factor.

DD FORM 1473 (1 NOV 65)

14 KEY WORDS	LINK A		LINK B		LINK C	
	ROLE	WT	ROLE	WT	ROLE	WT
lifting reentry vehicle						
recoverable spacecraft						
hypersonic flow						
aerodynamic heating						
surface temperature						
heat transfer						
boundary layer transition						
flow visualization						

AFSC
Arnold AFS Tenn